fractal and fractional

MDPI

Article

Stability and Hopf Bifurcation of a Delayed Fractional-Order ISR Rumor Propagation Model with Saturation Incidence

Ahmadjan Muhammadhaji * and Yahui Niu

College of Mathematics and Systems Science, Xinjiang University, Urumqi 830017, China
* Correspondence: ahmatjanam@aliyun.com

Abstract

With the widespread adoption of internet technology globally, the propagation of rumors on social networks has attracted significant scholarly attention. This paper discusses a type of fractional-order rumor propagation model incorporating a saturation effect. In this model, it is assumed that the state of an ignorant individual will invariably change upon contact with a spreader, while the influence of time delays is also considered. Subsequently, we focus on analyzing the existence of a Hopf bifurcation arising from the time delay between ignorant individuals and spreaders, along with the dynamic behavior of the model. Stability analysis is conducted using methods such as the fractional-order stability criterion. Finally, a series of numerical simulations validate our findings and reveal that increasing the fractional order reduces the critical bifurcation value, thereby shrinking the stability region. Therefore, the stability region of the model can be regulated by adjusting the fractional order.

Keywords: rumor propagation; fractional order; stability; Hopf bifurcation; Caputo fractional derivative; time delay

1. Introduction

Rumors refer to unverified information concerning subjects or events of public concern, typically spreading rapidly within society and involving diverse topics such as political, economic, and social incidents. Such information often carries emotional overtones or exaggerated elements, readily triggering public attention and discussion [1]. The spread of rumors is influenced by multiple factors, including social network structures, individual psychological factors, and information characteristics. With the rise of social media and the internet, the speed and scope of information dissemination have significantly increased. Concurrently, interpersonal interaction networks play a crucial role in rumor diffusion. Studying rumor propagation models holds substantial practical significance. These models not only enhance our understanding of how rumors spread but also provide theoretical support for maintaining social stability and safeguarding public safety. During emergencies, rumor propagation may induce public panic, thereby impeding emergency response efforts. Consequently, timely identification of and intervention in rumor dissemination are critical. Furthermore, such research outcomes offer scientific evidence for policymakers, enabling them to formulate more effective communication and intervention strategies to mitigate the negative societal impact of rumors.

In mathematical research on rumor propagation, the primary focus lies on analyzing the diffusion mechanisms of rumor information within populations and its societal impacts through the construction of rumor propagation models. Current scholarship has developed

Check for updates

Academic Editors: Faqiang Wang, Shaobo He and Hongbo Cao

Received: 22 July 2026
Revised: 2 October 2026
Accepted: 5 October 2026
Published: 8 October 2026

Copyright: © 2026 by the authors. Licensee MDPI, Basel, Switzerland. This article is an open access article distributed under the terms and conditions of the Creative Commons Attribution (CC BY) license.

a relatively profound understanding of the dynamical analysis of integer-order rumor propagation models. Numerous scholars have introduced complex mechanisms from multidimensional perspectives to construct models, yielding substantial and significant contributions. In their model construction, Zhao et al. [2] introduced the concept of propagation force—a fuzzy variable—into the classical Susceptible–Infected–Recovered (SIR) framework. By incorporating a fuzzy reproductive number, they computationally validated its theoretical rationality and explored rumor containment strategies. Pan et al. [3] proposed an SIDRW (Susceptibility–Infection–Refutation–Recovery–Medium) model, designating media as a distinct compartment. This formulation comprehensively integrates the impacts of media coverage and individual denial behavior on rumor propagation dynamics. Yin et al. [4] developed a two-stage rumor propagation dynamical model featuring innovative stratification of super-spreaders (agents with high rumor confidence) and ordinary spreaders. They further introduced supervisory cohorts and professional debunkers to capture the ecological diversity of public opinion landscapes.

Although extensive studies have been carried out on integer-order rumor propagation models, such models possess intrinsic drawbacks, especially in accurately describing the evolutionary features of rumor spreading. Consequently, fractional-order rumor propagation models have emerged as a promising research frontier, building upon the foundation of integer-order frameworks.

Fractional calculus constitutes a generalization of classical integer-order calculus, permitting derivatives and integrals of arbitrary real or complex orders. Its fundamental breakthrough lies in transcending the constraints of integer-order operations, thereby providing a mathematical framework to describe systems exhibiting complex characteristics such as memory effects and non-locality [5]. Fractional-order rumor propagation models demonstrate significant advantages in characterizing the complex dynamical behavior of rumor diffusion. Specifically, these models capture long-range memory dependence and temporally decaying memory intensity, reflecting human decision-making delays, where individuals postpone sharing rumors for hours or days. These models further simulate super-diffusion through spatial fractional operators (e.g., the Riesz fractional Laplace operator), replicating how rumors transcend geographical barriers via social media to trigger cross-regional outbreaks. Additionally, adaptive fractional orders quantify time-varying collective memory effects during emergent public opinion events. Such capabilities not only enhance real-world data fitting accuracy beyond integer-order frameworks but fundamentally reveal a critical departure from epidemic-spreading paradigms: the memory-entangled dynamics and spatial transcendence inherent to human behavioral propagation. This theoretical advancement constitutes an essential cornerstone for governing complex social systems [6–9]. In recent years, this field has garnered increasing scholarly attention. Ye and co-authors [10]. established a fractional-order rumor propagation model for multilingual contexts, analyzing the global asymptotic stability of equilibrium points using the Lyapunov function approach. Concurrently, Hou et al. [11] developed a stochastic fractional-order rumor propagation model incorporating time-varying nodal activity rates, and further conducted optimal control studies to identify effective intervention strategies.

Compared with these existing fractional-order rumor models, the present framework uniquely combines a Holling-type II saturation incidence rate, a single discrete time delay representing the rumor-fermentation period, and demographic dynamics (recruitment and attrition), and systematically analyzes how the fractional order α shifts the Hopf bifurcation threshold.

The remainder of this paper is organized as follows. Section 2 introduces a fractional-order ISR rumor propagation model with a time delay, incorporating a saturated incidence rate. This framework assumes that ignorant individuals inevitably undergo state transitions

upon exposure to rumors disseminated by spreaders; specifically, they either become rumor spreaders upon believing in the information or transition directly to the remover. Essential background information is presented. Section 3 focuses on the stability analysis of the equilibrium points (both rumor-free and positive equilibria) and examines the Hopf bifurcation dynamics inherent in the model. Section 4 provides the numerical validation of the principal conclusions, and Section 5 provides a concise synthesis of the study.

2. Model Formulation and Preliminaries

Based on the developmental context of rumor propagation models summarized in the introduction and existing relevant research results, this section constructs the dynamical model to be analyzed in this paper and lists the definitions and lemmas required throughout the full text.

In Ref. [12], Zhao et al. formulated the following integer-order rumor propagation model, which assumes that ignorant individuals will change their states once they receive rumors from spreaders:

$$\begin{cases} \dfrac{\mathrm{d}I(t)}{\mathrm{d}t} = -\bar{k}I(t)S(t), \\ \dfrac{\mathrm{d}S(t)}{\mathrm{d}t} = \lambda\bar{k}I(t)S(t) - \bar{k}S(t)(\gamma S(t) + \eta R(t)) - \delta S(t), \\ \dfrac{\mathrm{d}R(t)}{\mathrm{d}t} = (1-\lambda)\bar{k}I(t)S(t) + \bar{k}S(t)(\gamma S(t) + \eta R(t)) + \delta S(t). \end{cases} \tag{1}$$

Given that ignorant individuals possess inherent cognitive heterogeneity and naturally tend to accept information consistent with their inherent predispositions owing to disparate perspectives and attitudes, the assumption proposed by Zhao et al. accurately reflects real-world propagation scenarios. However, we observe that existing fractional-order rumor propagation models rarely account for such subtle behavioral characteristics and mostly simplify compartmental state transitions into linear piecewise processes.

On the other hand, in practical social-network scenarios, after ignorant individuals receive rumor information, there commonly exists a rumor-fermentation time lag: people do not immediately choose to spread or discard rumors; instead, psychological processing takes some time before state transition occurs. Standard instantaneous differential-equation models cannot represent such lagged behavioral responses; therefore, we adopt time-delay arguments in the contact incidence term to describe this delay effect.

Nevertheless, integer-order delayed models still follow Markov-type memory-less assumptions. Human social behaviors related to rumor propagation are history-dependent: individual attitudes and spreading decisions are influenced by previously received information, showing typical memory-dependent properties. Fractional-order derivatives provide a powerful mathematical tool to characterize such memory and non-local effects in dynamical systems [13–16]. Recent studies have compared different fractional operators—such as the Yang–Abdel–Cattani and Atangana–Baleanu derivatives—in modeling the transmission dynamics of fractional smoking epidemic models [17], and have demonstrated the applicability of new fractional derivative operators to non-local diffusion processes [18]. These studies support the use of fractional-order formulations for investigating memory effects and complex dynamics in delayed rumor-spreading models. For this reason, we further extend the integer-order delayed rumor-spreading system to its fractional-order counterpart.

Drawing on the above discussion and analysis, and inspired by the work of Zhao et al., we propose three key improvements to enhance the practical realism of the model: first, fractional-order operators coupled with time delays are adopted to characterize memory effects; second, saturated incidence terms are utilized instead of bilinear incidence functions

to more accurately reproduce the saturation phenomenon in real rumor spreading; and third, demographic dynamics of social network participation are integrated into the system, where Λ and μ represent the recruitment and exit rates of network users, and κ denotes the average degree of the social network.

Under the above framework, ignorant individuals who have contact with spreaders will switch to the spreader compartment with probability β or turn into removers with probability $1-\beta$. Meanwhile, spreaders spontaneously transform into removers at the recovery rate δ. The resulting dynamical model is formulated as follows:

$$\begin{cases} D^{\alpha}I(t) = \Lambda - \dfrac{\kappa I(t-\tau)S(t-\tau)}{1+bS(t-\tau)} - \mu I(t), \\ D^{\alpha}S(t) = \dfrac{\beta\kappa I(t-\tau)S(t-\tau)}{1+bS(t-\tau)} - \delta S(t) - \mu S(t), \\ D^{\alpha}R(t) = \dfrac{(1-\beta)\kappa I(t-\tau)S(t-\tau)}{1+bS(t-\tau)} + \delta S(t) - \mu R(t), \end{cases} \tag{2}$$

where $I(t)$ denotes the density of ignorant individuals at time t, $S(t)$ represents the density of spreader individuals, and $R(t)$ stands for the density of remover individuals (who neither believe nor disseminate rumors). Λ refers to the recruitment rate of new users entering the social network, κ is the average degree of the social network, and β denotes the probability that ignorant individuals receive and propagate rumors. δ is the probability that spreaders give up believing and spreading rumors, μ corresponds to the user attrition rate of the social network, τ denotes the time delay of the rumor-fermentation stage, and b is the saturation constant. All parameters in system (2) take positive values to satisfy their practical biological and social interpretations. The parameter α represents the fractional order satisfying $\alpha \in (0,1]$, and the system satisfies the following initial conditions:

$$I(\theta) = \phi_1(\theta), S(\theta) = \phi_2(\theta), R(\theta) = \phi_3(\theta),\ \phi_i(\theta) \geq 0,\ \theta \in [-\tau,\ 0]. \tag{3}$$

Furthermore, model (2) reduces to an integer-order system when $\alpha = 1$. This indicates that the integer-order rumor propagation model is merely a special case of its fractional-order counterpart. The state transition diagram corresponding to model (2) is illustrated in Figure 1.

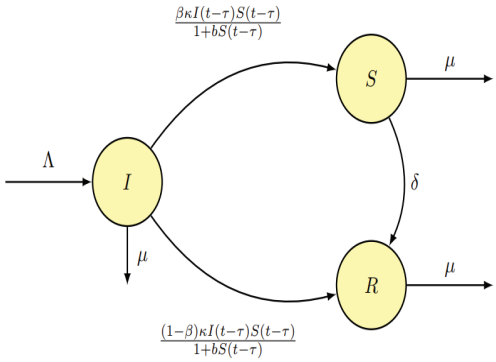


Figure 1. The state transition diagram.

Remark 1. *Following Ref. [12], the present model assumes that every ignorant individual under effective rumor exposure will leave the ignorant compartment and switch to spreader or remover with probability β or $1-\beta$, respectively. This is a strong behavioral simplification, as real-world agents may encounter rumors yet remain ignorant. Here, "exposure" refers to effective reception triggering psychological responses. This assumption guarantees only two equilibrium types (rumor-free and a unique positive equilibrium) and facilitates explicit stability and Hopf bifurcation analysis. Relaxing*

this assumption would alter the threshold condition and equilibrium structure, which deserves further study in future work.

Remark 2. *For the saturated incidence* $\frac{\kappa I(t-\tau)S(t-\tau)}{1+bS(t-\tau)}$*, saturation is imposed on the receiver population* S *to model limited cognitive attention, while spreader term* I *remains linear because spreaders can generate rumor content without intrinsic quantity constraints. Parameter* b *governs saturation strength: the limiting effective transmission rate equals* κ/b *for large* S*, and* $b = 0$ *reduces to bilinear incidence. Compared with alternative formulations, this Holling-type II form better captures the receiver-side bottleneck present in social media rumor propagation.*

Remark 3. *The Caputo fractional derivative in system (2) captures memory-dependent rumor-spreading behaviors. In contrast, with memory-ignorant local integer-order derivatives, this non-local operator assigns decaying power-law weights to historical states to model memory decay. Three factors motivate our choice of Caputo: (i) zero derivative for constants, consistent with compartment-model initial-condition rules; (ii) a compatible Laplace transform with delay term* $e^{-\tau s}$*, facilitating the Section 3 characteristic equation analysis; and (iii) widespread usage in fractional epidemic-rumor studies for easy literature comparison. The parameter* $\alpha \in (0, 1]$ *quantifies memory strength: smaller* α *means stronger memory, and* $\alpha \to 1$ *recovers the memory-free integer-order limit. Consistent with numerical results, the Hopf bifurcation threshold* τ_0 *falls as* α *rises; stronger memory enlarges the stability region. Notably,* α *and* τ *play separate and complementary roles:* τ *represents short-term psychological fermentation lag after rumor exposure, whereas* α *embodies long-term cumulative memory; only their combination reproduces both effects simultaneously.*

Remark 4. *The mathematical novelties of system (2) are three-fold. First, unlike the delay-free integer-order bilinear incidence model [12] and existing fractional-order rumor models missing delay or saturation, our system jointly integrates the Caputo fractional derivative, delayed contact incidence and Holling-type II saturation. This triple coupling produces a fractional delayed quasi-polynomial characteristic equation irreducible to those in [9,12]. In addition, building upon the fractional-order delayed framework of Niu and Muhammadhaji [9], the present model differs in three key aspects: it adopts a Holling-type II saturation incidence instead of bilinear incidence, incorporates demographic recruitment and attrition, and focuses on the ISR compartment structure. These modifications lead to a different characteristic equation and yield the new finding that the fractional order systematically shifts the Hopf bifurcation threshold. Second, we prove solution existence, uniqueness, positivity and boundedness using history-space Lipschitz estimates and the Mittag-Leffler function; these results do not trivially follow from integer-order theory. Third, we obtain the fractional-dependent Hopf bifurcation threshold* τ_0 *and analytically show that* α *modulates the system's stability region, revealing a novel mathematical mechanism unavailable in integer-order or delay-free fractional rumor models.*

For the convenience of subsequent theoretical derivations, we provide all necessary definitions and lemmas in this section, consisting of one definition and two lemmas.

Definition 1 ([5])**.** *The Caputo fractional derivative is defined as*

$$ {}_{t_0}^{C}D_t^{\alpha} f(x) = \frac{1}{\Gamma(n-\alpha)} \int_{t_0}^{t} \frac{f^{(n)}(\tau)}{(t-\tau)^{\alpha+1-n}} \mathrm{d}\tau, $$

where n *denotes a positive integer,* α *represents the order of the fractional derivative satisfying* $n-1 < \alpha < n$*, and* $\Gamma(\cdot)$ *is the Gamma function with* $\Gamma(s) = \int_0 \varrho^{\infty} t^{s-1} e^{-t} dt$*.*

Lemma 1 ([14]). *Consider an n-dimensional linear fractional-order system with multiple time delays:*

$$\begin{cases} {}_{t_0}^{C}D_t^{\alpha_1} z_1(t) = b_{11}z_1(t-\tau_{11}) + b_{12}z_2(t-\tau_{12}) + \cdots + b_{1n}z_n(t-\tau_{1n}), \\ {}_{t_0}^{C}D_t^{\alpha_2} z_2(t) = b_{21}z_1(t-\tau_{21}) + b_{22}z_2(t-\tau_{22}) + \cdots + b_{2n}z_n(t-\tau_{2n}), \\ \qquad\qquad \vdots \\ {}_{t_0}^{C}D_t^{\alpha_n} z_n(t) = b_{n1}z_1(t-\tau_{n1}) + b_{n2}z_2(t-\tau_{n2}) + \cdots + b_{nn}z_n(t-\tau_{nn}), \end{cases}$$

where $\alpha_i \in (0,1]$ represents the fractional order corresponding to the i-th state variable of the system, $\boldsymbol{z}(t) = (z_1(t), z_2(t), \ldots, z_n(t))$ denotes the state vector, and $\tau_{ij} > 0$ $(i,j = 1,2,\ldots,n)$ represents the time delay. The initial condition of the system is given by

$$z_i(t) = \phi_i(t), \quad t \in [-\tau_{\max}, 0], \quad i = 1,2,\ldots,n,$$

where $\tau_{\max} = \max_{1\le i,j\le n}\{\tau_{ij}\}$. Let the coefficient matrix of system (3) be $\boldsymbol{B} = [b_{ij}]_{n\times n} \in \mathbb{R}^{n\times n}$. Then the characteristic matrix $\triangle(k)$ of the system is defined as

$$\triangle(k) = \begin{pmatrix} k^{\alpha_1} - b_{11}e^{-k\tau_{11}} & -b_{12}e^{-k\tau_{12}} & \cdots & -b_{1n}e^{-k\tau_{1n}} \\ -b_{21}e^{-k\tau_{21}} & k^{\alpha_2} - b_{22}e^{-k\tau_{22}} & \cdots & -b_{2n}e^{-k\tau_{2n}} \\ \vdots & \vdots & \ddots & \vdots \\ -b_{n1}e^{-k\tau_{n1}} & -b_{n2}e^{-k\tau_{n2}} & \cdots & k^{\alpha_n} - b_{nn}e^{-k\tau_{nn}} \end{pmatrix}.$$

Lemma 2 ([15]). *Consider the linear autonomous Caputo fractional-order system*

$${}_{0}^{C}D_t^{\alpha} X(t) = \boldsymbol{A}X(t),$$

where $\boldsymbol{A} \in \mathbb{R}^{n\times n}$ and $\alpha \in (0,1]$. This system is asymptotically stable if and only if every eigenvalue λ of matrix $\boldsymbol{A}$ satisfies

$$|\arg(\lambda)| > \frac{\alpha\pi}{2}.$$

Otherwise, the system is unstable.

3. Main Results

3.1. Existence, Uniqueness, Positivity and Boundedness of Solutions

In this section, we present the results concerning the existence, uniqueness, positivity, and boundedness of solutions for system (2).

Theorem 1. *The fractional-order delayed system (2) subject to the initial conditions (3) admits a unique continuous solution $(I(t), S(t), R(t))$ for all $t \ge 0$.*

Proof. Define the state-history vector $\boldsymbol{x}_t(\theta) = \big(I(t+\theta),\, S(t+\theta),\, R(t+\theta)\big)$, $\theta \in [-\tau, 0]$, and the right-hand-side vector-valued function $\boldsymbol{f} : [0,+\infty) \times C([-\tau,0],\mathbb{R}^3) \to \mathbb{R}^3$ as

$$\boldsymbol{f}(t,\boldsymbol{x}_t) = \begin{pmatrix} \Lambda - \dfrac{\kappa I(t-\tau)S(t-\tau)}{1+bS(t-\tau)} - \mu I(t) \\ \dfrac{\beta\kappa I(t-\tau)S(t-\tau)}{1+bS(t-\tau)} - (\delta+\mu)S(t) \\ \dfrac{(1-\beta)\kappa I(t-\tau)S(t-\tau)}{1+bS(t-\tau)} + \delta S(t) - \mu R(t) \end{pmatrix}.$$

Our system (2) can be rewritten in the compact form ${}^{C}D_t^{\alpha}\boldsymbol{x}(t) = \boldsymbol{f}(t,\boldsymbol{x}_t)$, $t \ge 0$, $\boldsymbol{x}(\theta) = \big(\phi_1(\theta), \phi_2(\theta), \phi_3(\theta)\big)$, $\theta \in [-\tau, 0]$.

First, the mapping $\boldsymbol{f}(t, \boldsymbol{x}_t)$ is continuous with respect to t and the history state $\boldsymbol{x}_t$, because all terms are combinations of rational functions with denominator $1 + bS(t-\tau) > 0$ for $S(t-\tau) \geq 0$, and all algebraic operations preserve continuity.

Next, we verify that $\boldsymbol{f}$ satisfies the Lipschitz condition on any compact subset of the phase space. Take any bounded closed set $\Omega \subset C([-\tau, 0], \mathbb{R}^3)$. For two history functions $\boldsymbol{x}_t, \boldsymbol{y}_t \in \Omega$, denote

$$I_1 = I(t-\tau),\ S_1 = S(t-\tau),\ R_1 = R(t),$$
$$I_2 = \tilde{I}(t-\tau),\ S_2 = \tilde{S}(t-\tau),\ R_2 = \tilde{R}(t).$$

Examine the nonlinear term $F(u, v) = \frac{\kappa uv}{1+bv}$. Compute its partial derivatives: $\frac{\partial F}{\partial u} = \frac{\kappa v}{1+bv}$, $\frac{\partial F}{\partial v} = \frac{\kappa u}{(1+bv)^2}$. On the bounded set Ω, variables u, v are bounded, so partial derivatives are uniformly bounded. Thus, there exists a constant $L_0 > 0$ such that $|F(u_1, v_1) - F(u_2, v_2)| \leq L_0\big(|u_1 - u_2| + |v_1 - v_2|\big)$. Each component of $\boldsymbol{f}$ consists of this nonlinear term plus linear terms $-\mu I$, $-(\delta + \mu)S$, $-\mu R$, and δS. Linear terms are globally Lipschitz. Therefore, there exists a Lipschitz constant $L > 0$, such that $\big\|\boldsymbol{f}(t, \boldsymbol{x}_t) - \boldsymbol{f}(t, \boldsymbol{y}_t)\big\|_{\mathbb{R}^3} \leq L \big\|\boldsymbol{x}_t - \boldsymbol{y}_t\big\|_{C([-\tau,0],\mathbb{R}^3)}$, where $\|\cdot\|_C$ is the supremum norm for continuous history functions.

Since $\boldsymbol{f}$ is continuous and satisfies the Lipschitz condition on compact sets, applying the existence-uniqueness theorem for Caputo fractional delay differential equations (see Deng and Li, 2007, Lemma 14 in [14]), we conclude that the initial-value problem of system (2) possesses a unique continuous solution defined for all $t \geq 0$. This completes the proof. □

Theorem 2. *For system (2) subject to non-negative initial conditions (3), every component of its solution satisfies* $I(t) \geq 0, \quad S(t) \geq 0, \quad R(t) \geq 0, \quad \forall\, t \geq 0$. *Furthermore, all solutions are uniformly bounded. In particular,*

$$\limsup_{t \to +\infty} \big(I(t) + S(t) + R(t)\big) \leq \frac{\Lambda}{\mu}.$$

Proof. First, we prove the boundedness of solutions. We use proof by contradiction. From the existence-uniqueness theorem, the solution $(I(t), S(t), R(t))$ is continuous for $t \geq -\tau$. The initial conditions give $I(\theta) \geq 0,\ S(\theta) \geq 0,\ R(\theta) \geq 0,\ \theta \in [-\tau, 0]$. Assume for contradiction that at least one variable becomes negative for some $t > 0$. Define the first blow-up time $t^* = \inf\big\{t > 0 \,\big|\, I(t) < 0 \text{ or } S(t) < 0 \text{ or } R(t) < 0\big\}$. By the continuity of solutions, we have $I(t^*) \geq 0, \quad S(t^*) \geq 0, \quad R(t^*) \geq 0$, and at least one equality holds. For all $t \in [0, t^*)$, we have $I(t) \geq 0, S(t) \geq 0, R(t) \geq 0$. Consequently, for $t \in [\tau, t^* + \tau)$, we get $I(t-\tau) \geq 0, S(t-\tau) \geq 0$.

We now consider three possible cases:

Case 1: $I(t^*) = 0$. For $t \in [0, t^*)$, $I(t) \geq 0$. Evaluate the Caputo fractional derivative at $t = t^*$: ${}^C D_t^\alpha I(t^*) = \Lambda - \frac{\kappa\, I(t^*-\tau)S(t^*-\tau)}{1+bS(t^*-\tau)} - \mu I(t^*)$. Since $I(t^*) = 0$, $\Lambda > 0$, and the nonlinear term is non-negative, ${}^C D_t^\alpha I(t^*) = \Lambda - \frac{\kappa\, I(t^*-\tau)S(t^*-\tau)}{1+bS(t^*-\tau)} \geq 0$. By the property of the Caputo fractional derivative, if $I(t^*) = 0$ and ${}^C D_t^\alpha I(t^*) \geq 0$, $I(t)$ cannot cross to negative values immediately after t^*. This contradicts the definition of t^*.

Case 2: $S(t^*) = 0$. Then ${}^C D_t^\alpha S(t^*) = \frac{\beta\kappa\, I(t^*-\tau)S(t^*-\tau)}{1+bS(t^*-\tau)} - (\delta+\mu)S(t^*) = \frac{\beta\kappa\, I(t^*-\tau)S(t^*-\tau)}{1+bS(t^*-\tau)} \geq 0$. Similarly, $S(t^*) = 0$ together with ${}^C D_t^\alpha S(t^*) \geq 0$ implies that $S(t)$ cannot turn negative for $t > t^*$. Contradiction.

Case 3: $R(t^*) = 0$. ${}^C D_t^\alpha R(t^*) = \frac{(1-\beta)\kappa\, I(t^*-\tau)S(t^*-\tau)}{1+bS(t^*-\tau)} + \delta S(t^*) - \mu R(t^*)$. Since $R(t^*) = 0$ and all other terms on the right-hand side are non-negative, we obtain ${}^C D_t^\alpha R(t^*) \geq 0$. Hence $R(t)$ cannot become negative for $t > t^*$. Contradiction.

All three cases lead to contradiction. Therefore, our assumption is false. We conclude $I(t) \geq 0,\ S(t) \geq 0,\ R(t) \geq 0,\ \forall\, t \geq 0$.

Next, we turn to the uniform boundedness of solutions. Define the total population variable $N(t) = I(t) + S(t) + R(t)$. Sum up the three equations of system (2):

$$\begin{aligned} {}^{C}D_t^{\alpha} N(t) &= {}^{C}D_t^{\alpha} I(t) + {}^{C}D_t^{\alpha} S(t) + {}^{C}D_t^{\alpha} R(t) \\ &= \Lambda - \mu I(t) - (\delta + \mu) S(t) + \delta S(t) - \mu R(t) \\ &= \Lambda - \mu\big(I(t) + S(t) + R(t)\big) \\ &= \Lambda - \mu N(t). \end{aligned}$$

We obtain a simple fractional-order differential equation: ${}^{C}D_t^{\alpha} N(t) = \Lambda - \mu N(t)$. Since $I(t), S(t), R(t) \geq 0$, we have $N(t) \geq 0$. Solving this Caputo fractional-order linear differential equation, one can obtain $N(t) = \frac{\Lambda}{\mu} + \Big(N(0) - \frac{\Lambda}{\mu}\Big) E_{\alpha}\big(-\mu t^{\alpha}\big)$, where $E_{\alpha}(\cdot)$ denotes the Mittag-Leffler function. Recall that $E_{\alpha}(-\mu t^{\alpha}) \to 0$ as $t \to +\infty$. It follows that $\limsup_{t \to +\infty} N(t) \leq \frac{\Lambda}{\mu}$. Thus, $I(t)$, $S(t)$ and $R(t)$ are uniformly bounded for all $t \geq 0$. The proof is complete. □

3.2. Stability Analysis

Given its practical significance, we further investigate the stability and bifurcation characteristics of the positive equilibrium of the proposed model. The equilibrium points of system (2) are solved as follows:

(i) The rumor-free equilibrium point is $E_0 = (\frac{\Lambda}{\mu}, 0, 0)$.

(ii) The rumor-spreading equilibrium point is $E^* = (I^*, S^*, R^*)$, where

$$\begin{aligned} I^* &= \frac{(\delta + \mu)(1 + bS^*)}{\beta\kappa}, \\ S^* &= \frac{\beta\Lambda\kappa - \mu(\delta + \mu)}{(\delta + \mu)(\kappa + \mu b)}, \\ R^* &= \frac{1}{\mu}\left[\frac{(1 - \beta)\kappa I^* S^*}{1 + bS^*} + \delta S^*\right]. \end{aligned}$$

We next derive and analyze the conditions for the positivity of the rumor-spreading equilibrium.

Substituting the positive equilibrium $E^* = (I^*, S^*, R^*)$ into system (2), we can directly derive

$$\frac{\beta\kappa I^*}{1 + bS^*} = \delta + \mu.$$

Rearranging the above equation, we can obtain

$$I^* = \frac{(\delta + \mu)(1 + bS^*)}{\beta\kappa}.$$

Define

$$G = \frac{\kappa I^* S^*}{1 + bS^*},$$

then we have

$$\Lambda = G + \mu I^*, \tag{4}$$

and

$$\beta G = (\delta + \mu) S^*.$$

Thus,

$$G = \frac{(\delta+\mu)S^*}{\beta}, \Lambda = \frac{(\delta+\mu)S^*}{\beta} + \mu I^*.$$

Substituting the above equation into (4), it is easy to obtain

$$\Lambda = \frac{(\delta+\mu)S^*}{\beta} + \frac{\mu(\delta+\mu)(1+bS^*)}{\beta\kappa}.$$

Rearranging terms, we have

$$S^* = \frac{\beta\Lambda\kappa - \mu(\delta+\mu)}{(\delta+\mu)(\kappa+\mu b)}. \tag{5}$$

Since all parameters of system (2) are positive to satisfy practical biological interpretations, it follows from (5) that $S^* > 0$ if and only if hypothesis (H_1) holds, where

$$(H_1) : \frac{\Lambda\beta}{\delta+\mu} > \frac{\mu}{\kappa}. \tag{6}$$

It is easy to observe that $I^* > 0$ and $R^* > 0$ if $S^* > 0$. In other words, the equilibrium solutions of system (2) are all positive in this scenario.

Based on the above analysis and derivations, we arrive at the following corollary.

Corollary 1. *Under assumption (H_1), system (2) admits a unique positive equilibrium E^*.*

From assumption (H_1) and with simple algebraic manipulation yields: $\frac{\Lambda\beta}{\delta+\mu} > \frac{\mu}{\kappa} \iff \beta\kappa\Lambda > \mu(\delta+\mu) \iff \mathcal{R}_0 = \frac{\beta\kappa\Lambda}{\mu(\delta+\mu)} > 1$, where $\mathcal{R}_0$ is the basic rumor reproduction number.

From a modeling perspective, $\mathcal{R}_0$ describes the average number of new rumor spreaders produced by a single spreader when the whole population is ignorant. The threshold condition $\mathcal{R}_0 = 1$ separates two dynamical regimes: (i) If $\mathcal{R}_0 < 1$, the rumor-free equilibrium E_0 is locally asymptotically stable and the rumor will eventually die out. (ii) If $\mathcal{R}_0 > 1$, E_0 becomes unstable and a unique positive rumor-spreading equilibrium E^* emerges.

Regarding the stability of the rumor-free equilibrium E_0 for system (2), we have the following result.

Theorem 3. *The rumor-free equilibrium E_0 of system (2) is locally asymptotically stable provided that $\mathcal{R}_0 < 1$ and unstable if $\mathcal{R}_0 > 1$.*

Proof. We first derive the Jacobian matrix of system (2) at E_0.

$$J(E_0) = \begin{pmatrix} -\mu & -\kappa\frac{\Lambda}{\mu} & 0 \\ 0 & \beta\kappa\frac{\Lambda}{\mu} - \delta - \mu & 0 \\ 0 & (1-\beta)\kappa\frac{\Lambda}{\mu} + \delta & -\mu \end{pmatrix}.$$

To calculate the eigenvalues at the equilibrium, we construct the characteristic matrix Θ.

$$\Theta = \begin{pmatrix} \lambda+\mu & \kappa\frac{\Lambda}{\mu} & 0 \\ 0 & \lambda - \beta\kappa\frac{\Lambda}{\mu} + \delta + \mu & 0 \\ 0 & -(1-\beta)\kappa\frac{\Lambda}{\mu} - \delta & \lambda+\mu \end{pmatrix}.$$

We then derive the characteristic equation of system (2) as follows:

$$(\lambda+\mu)^2(\lambda - \beta\kappa\frac{\Lambda}{\mu} + \delta + \mu) = 0. \tag{7}$$

By solving Equation (7), we finally derive the eigenvalues of system (2) at E_0.

$$\lambda_{1,2} = -\mu,\ \lambda_3 = \beta\kappa\frac{\Lambda}{\mu} - \delta - \mu.$$

When $\mathcal{R}_0 < 1$, i.e., $\dfrac{\beta\kappa\Lambda}{\mu} < \delta + \mu$, the eigenvalues of system (2) evaluated at E_0 are

$$\lambda_{1,2} = -\mu, \quad \lambda_3 = \frac{\beta\kappa\Lambda}{\mu} - (\delta + \mu) < 0.$$

All three eigenvalues are real and negative, which yields

$$|\arg(\lambda_i)| = \pi > \frac{\alpha\pi}{2}, \quad i = 1, 2, 3,$$

for any $\alpha \in (0, 1]$. Consequently, the fractional-order spectral stability condition given in Lemma 2 is satisfied, so that E_0 is locally asymptotically stable. When $\mathcal{R}_0 > 1$, we have $\lambda_3 > 0$, hence $|\arg(\lambda_3)| = 0 < \dfrac{\alpha\pi}{2}$, and E_0 becomes unstable. This completes the proof. □

We have analyzed the stability of the rumor-free equilibrium E_0 in the preceding section. We now turn our attention to the rumor-spreading equilibrium E^*. To distinguish delay-triggered dynamical phenomena, we first examine the undelayed case $\tau = 0$, and further analyze the stability and bifurcation characteristics of the system when $\tau > 0$.

Let $\bar{I}(t) = I(t) - I^*$, $\bar{S}(t) = S(t) - S^*$, $\bar{R}(t) = R(t) - R^*$. Linearizing system (2) around the equilibrium yields the following linearized system.

$$\begin{cases} D^\alpha \bar{I}(t) = a_{11}\bar{I}(t-\tau) + a_{12}\bar{S}(t-\tau) + b_{11}\bar{I}(t), \\ D^\alpha \bar{S}(t) = a_{21}\bar{I}(t-\tau) + a_{22}\bar{S}(t-\tau) + b_{21}\bar{S}(t), \\ D^\alpha \bar{R}(t) = a_{31}\bar{I}(t-\tau) + a_{32}\bar{S}(t-\tau) + b_{31}\bar{S}(t) + b_{32}\bar{R}(t), \end{cases} \tag{8}$$

where

$$\begin{aligned} a_{11} &= -\frac{\kappa S^*}{1+bS^*},\ a_{12} = -\frac{\kappa I^*}{(1+bS^*)^2},\ b_{11} = -\mu, \\ a_{21} &= \frac{\beta\kappa S^*}{1+bS^*},\ a_{22} = \frac{\beta\kappa I^*}{(1+bS^*)^2},\ b_{21} = -(\delta+\mu), \\ a_{31} &= \frac{(1-\beta)\kappa S^*}{1+bS^*},\ a_{32} = \frac{(1-\beta)\kappa I^*}{(1+bS^*)^2},\ b_{31} = \delta, b_{32} = -\mu. \end{aligned}$$

The linearized system (8) is derived via Taylor series expansion of the right-hand-side functions of the nonlinear system (2) around the positive equilibrium. All higher-order infinitesimal terms are discarded, so that system (8) gives the local linear approximation of the original nonlinear system (2) near this equilibrium point.

To simplify calculations, system (8) serves as a linear approximation to system (2). Applying the Laplace transform to both sides of system (8), we derive its characteristic matrix with the aid of Lemma 1.

$$\Delta(s) = \begin{pmatrix} s^\alpha - a_{11}e^{-\tau s} - b_{11} & -a_{12}e^{-\tau s} & 0 \\ -a_{21}e^{-\tau s} & s^\alpha - a_{22}e^{-\tau s} - b_{21} & 0 \\ -a_{31}e^{-\tau s} & -a_{32}e^{-\tau s} - b_{31} & s^\alpha - b_{32} \end{pmatrix}.$$

We compute the characteristic roots of system (8) from the characteristic determinant (9), which allows us to analyze the dynamical properties of system (2) indirectly.

$$\det(\Delta(s)) = \begin{vmatrix} s^{\alpha} - a_{11}e^{-\tau s} - b_{11} & -a_{12}e^{-\tau s} & 0 \\ -a_{21}e^{-\tau s} & s^{\alpha} - a_{22}e^{-\tau s} - b_{21} & 0 \\ -a_{31}e^{-\tau s} & -a_{32}e^{-\tau s} - b_{31} & s^{\alpha} - b_{32} \end{vmatrix} = 0. \tag{9}$$

By Lemma 2, system (2) is locally asymptotically stable at E^* if and only if every characteristic root λ of the linearized system (8) satisfies the fractional-order spectral condition $|\arg(\lambda)| > \frac{\alpha\pi}{2}$. Conversely, if there exists a characteristic root with $|\arg(\lambda)| < \frac{\alpha\pi}{2}$, then E^* is unstable. When $|\arg(\lambda)| = \frac{\alpha\pi}{2}$, the equilibrium lies on the stability boundary, corresponding to the critical state at which Hopf bifurcations emerge.

Rearranging and simplifying the characteristic Equation (9) containing delay terms, we derive

$$B_1(s) + B_2(s)e^{-\tau s} = 0, \tag{10}$$

where

$$B_1(s) = S^{3\alpha} + A_1S^{2\alpha} + A_2S^{\alpha} + A_3,$$
$$B_2(s) = A_4S^{2\alpha} + A_5S^{\alpha} + A_6,$$

and

$$A_1 = -b_{21} - b_{11} - b_{32},$$
$$A_2 = b_{11}b_{21} + b_{21}b_{32} + b_{11}b_{32},$$
$$A_3 = -b_{11}b_{21}b_{32},$$
$$A_4 = -a_{22} - a_{11},$$
$$A_5 = a_{11}b_{21} + a_{22}b_{11} + a_{22}b_{32} + a_{11}b_{32},$$
$$A_6 = -a_{11}b_{21}b_{32} - a_{22}b_{11}b_{32}.$$

Furthermore, it can be further observed from Table 1 that $A_1, \ldots, A_6$ can be independently verified. It should be emphasized that, for the fractional-order system (2), the stability of E^* is determined by the fractional-order spectral condition $|\arg(s)| > \alpha\pi/2$ rather than by the sign of $\mathrm{Re}(s)$ alone. The subsequent Hopf bifurcation analysis is therefore carried out directly on the imaginary axis $s = i\omega$, which is exactly the boundary $|\arg(s)| = \pi/2$ of the fractional-order stability region.

Table 1. Coefficient mapping table.

Term in $\det\Theta(s)$	Coefficient	Expression in Terms of a_{ij}, b_{ij}
$s^{3\alpha}$	1	—
$s^{2\alpha}$	A_1	$-b_{21} - b_{11} - b_{32}$
s^{α}	A_2	$b_{11}b_{21} + b_{21}b_{32} + b_{11}b_{32}$
constant	A_3	$-b_{11}b_{21}b_{32}$
$s^{2\alpha}e^{-s\tau}$	A_4	$-a_{22} - a_{11}$
$s^{\alpha}e^{-s\tau}$	A_5	$a_{11}b_{21} + a_{22}b_{11} + a_{22}b_{32} + a_{11}b_{32}$
$e^{-s\tau}$	A_6	$-a_{11}b_{21}b_{32} - a_{22}b_{11}b_{32}$

Considering the undelayed case $\tau = 0$ and substituting $\lambda = S^{\alpha}$, we rationalize the characteristic Equation (10) and rewrite it as Equation (11).

$$\lambda^3 + c_1\lambda^2 + c_2\lambda + c_3 = 0, \tag{11}$$

where

$$c_1 = A_1 + A_4,$$
$$c_2 = A_2 + A_5,$$
$$c_3 = A_3 + A_6.$$

We derive the Hurwitz determinants associated with characteristic Equation (11).

$$\Delta = \begin{vmatrix} c_1 & 1 & 0 \\ c_3 & c_2 & c_1 \\ 0 & 0 & c_3 \end{vmatrix}.$$

We then analyze the stability of the system governed by Equation (11) using the Routh–Hurwitz stability criterion. The system is clearly stable provided that Assumptions (H_1) and (H_2) hold, where

$$(H_2) : \Delta_1 > 0, \Delta_2 > 0, \Delta_3 > 0,$$

and

$$\Delta_1 = |c_1|,\ \Delta_2 = \begin{vmatrix} c_1 & 1 \\ c_3 & c_2 \end{vmatrix},\ \Delta_3 = \begin{vmatrix} c_1 & 1 & 0 \\ c_3 & c_2 & c_1 \\ 0 & 0 & c_3 \end{vmatrix}.$$

From the above analyses and derivations, we draw the following conclusions.

Theorem 4. *Suppose $\tau = 0$, $\alpha \in (0, 1]$, and assumptions (H_1) and (H_2) hold for system (2). Then the positive equilibrium E^* of system (2) is locally asymptotically stable in the fractional-order sense, i.e., all roots z_1, z_2, z_3 of the characteristic Equation (11) satisfy*

$$|\arg(z_i)| > \frac{\alpha\pi}{2}, \quad i = 1, 2, 3.$$

Proof. When $\tau = 0$, the characteristic equation $\det(s^\alpha I - J) = 0$, upon setting $\lambda = s^\alpha$, reduces to the cubic polynomial $\det(\lambda I - J) = \lambda^3 + c_1\lambda^2 + c_2\lambda + c_3 = 0$, whose roots z_1, z_2, z_3 are precisely the eigenvalues of the Jacobian matrix J evaluated at E^*. Under assumptions (H_1) and (H_2), the Routh–Hurwitz criterion ensures that all eigenvalues satisfy $\mathrm{Re}(z_i) < 0$, i.e., they lie in the open left half-plane, which implies $|\arg(z_i)| > \frac{\pi}{2}$, $i = 1, 2, 3$. Since the fractional order $\alpha \in (0, 1]$, we have $\alpha\pi/2 \leq \pi/2$. Consequently, $|\arg(z_i)| > \frac{\pi}{2} \geq \frac{\alpha\pi}{2}$, which satisfies the asymptotic stability condition of Lemma 2. By Lemma 2, the fractional-order system (2) is locally asymptotically stable at E^*.

We note that this is a sufficient, but not necessary, condition: for $\alpha < 1$, the fractional stability sector $|\arg(\lambda)| > \alpha\pi/2$ is strictly wider than the left half-plane, so the system may remain stable even if some eigenvalues possess small positive real parts. The Routh–Hurwitz criterion provides a conservative yet analytically tractable sufficient condition. This completes the proof. □

3.3. Hopf Bifurcation

To explore the Hopf bifurcation behavior of the system, we next analyze the general case with positive time delay $\tau > 0$.

Set $s = i\omega = \omega e^{\frac{\pi i}{2}}$ and substitute this expression into Equation (10) for $\tau > 0$. We then derive

$$(\cos w\tau - i \sin w\tau) = -\frac{B_1(iw)}{B_2(iw)}, B_2(iw) \neq 0.$$

Separating the real and imaginary parts, we arrive at the following relation:

$$\cos w\tau = -\frac{K_1 \times K_3 + K_2 \times K_4}{K_3^2 + K_4^2},$$
$$\sin w\tau = \frac{-K_1 \times K_4 + K_2 \times K_3}{K_3^2 + K_4^2},$$

where

$$K_1 = \mathrm{Re}[B_1(iw)] = \omega^{3\alpha}\cos\frac{3\pi\alpha}{2} + A_1\omega^{2\alpha}\cos\pi\alpha + A_2\omega^{\alpha}\cos\frac{\pi\alpha}{2} + A_3,$$
$$K_2 = \mathrm{Im}[B_1(iw)] = \omega^{3\alpha}\sin\frac{3\pi\alpha}{2} + A_1\omega^{2\alpha}\sin\pi\alpha + A_2\omega^{\alpha}\sin\frac{\pi\alpha}{2},$$
$$K_3 = \mathrm{Re}[B_2(iw)] = A_4\omega^{2\alpha}\cos\pi\alpha + A_5\omega^{\alpha}\cos\frac{\pi\alpha}{2} + A_6,$$
$$K_4 = \mathrm{Im}[B_2(iw)] = A_4\omega^{2\alpha}\sin\pi\alpha + A_5\omega^{\alpha}\sin\frac{\pi\alpha}{2}.$$

Using the identity $\cos^2(\tau\omega) + \sin^2(\tau\omega) = 1$, we arrive at the following result

$$g_0\omega^{6\alpha} + g_1\omega^{5\alpha} + g_2\omega^{4\alpha} + g_3\omega^{3\alpha} + g_4\omega^{2\alpha} + g_5\omega^{\alpha} + g_6 = 0, \tag{12}$$

where

$$g_0 = 1,$$
$$g_1 = 2A_1\cos\pi\alpha\cos\frac{3\pi\alpha}{2} + 2A_1\sin\pi\alpha\sin\frac{\pi\alpha}{2},$$
$$g_2 = A_1^2 - A_4^2 + 2A_2\cos\frac{\pi\alpha}{2}\cos\frac{3\pi\alpha}{2} + 2A_2\sin\frac{\pi\alpha}{2}\sin\frac{3\pi\alpha}{2},$$
$$g_3 = 2A_3\cos\frac{3\pi\alpha}{2} + 2A_1A_2\cos\pi\alpha\cos\frac{\pi\alpha}{2} - 2A_4A_5\cos\pi\alpha\cos\frac{\pi\alpha}{2} + 2A_1A_2\sin\pi\alpha\sin\frac{\pi\alpha}{2} - 2A_4A_5\sin\pi\alpha\sin\frac{\pi\alpha}{2},$$
$$g_4 = A_2^2 - A_5^2 + 2A_1A_3\cos\pi\alpha - 2A_4A_6\cos\pi\alpha,$$
$$g_5 = 2A_2A_3\cos\frac{\pi\alpha}{2} - 2A_5B_6\cos\frac{\pi\alpha}{2},$$
$$g_6 = A_3^2 - A_6^2.$$

For ease of analysis, set $h = \omega^{\alpha}$. This yields the continuous function $f(h)$ given below:

$$f(h) = g_0h^6 + g_1h^5 + g_2h^4 + g_3h^3 + g_4h^2 + g_5h + g_6. \tag{13}$$

From Equation (13), we derive

$$f'(h) = 6h^5 + 5g_1h^4 + 4g_2h^3 + 3g_3h^2 + 2g_4h + g_5.$$

We make the following assumption:

$$(\mathrm{H}_3) : g_6 < 0.$$

To analyze the Hopf bifurcation of the system, we first introduce the following lemma.

Proposition 1. *The following conclusions can be derived from Equation (13):*

(i) If $g_i \geq 0$ for all $i = 0, 1, \ldots, 6$, the continuous function $f(h)$ admits no positive real roots.

(ii) Under assumption (H_3), Equation (13) possesses a positive root, which implies that system (10) has a purely imaginary characteristic root.

Proof. (i) Given $g_i \geq 0$ for $i = 0, 1, \ldots, 6$, we deduce $f'(h) > 0$ for all $h > 0$. Thus, $f(h)$ is strictly monotonically increasing on $h > 0$. Moreover, as $f(0) = g_6 \geq 0$, Equation (13) has no positive roots.

(ii) Since $f(h)$ is continuous and Assumption (H_3) holds, we readily obtain $f(0) = g_6 < 0$ and $\lim_{h\to+\infty} f(h) > 0$. By the Intermediate Value Theorem, $f(h)$ has at least one positive root h_0. Consequently, Equation (12) admits a positive solution $\omega_0 = h_0^{1/\alpha}$, which means characteristic Equation (10) possesses a pair of purely imaginary roots $\pm i\omega_0$. This completes the proof of Proposition 1. □

To derive the conditions for the onset of Hopf bifurcation, we introduce the following assumption:

$$(H_4) \quad \Theta_1\Theta_3 + \Theta_2\Theta_4 > 0$$

The parameters Θ_1, Θ_2, Θ_3 and Θ_4 are defined in the proof of the subsequent lemma. Relying on the foregoing theorem, we establish the key lemma below.

Lemma 3. *If assumption (H_4) holds, let $s(\tau_0) = \phi(\tau_0) + i\omega(\tau_0)$ be a root of Equation (10) satisfying $\phi(\tau_0) = 0$ and $\omega(\tau_0) > 0$. Then the following transversality condition is satisfied:*

$$\mathrm{Re}\left[\frac{ds}{d\tau}\right]\Big|_{\tau=\tau_0} > 0.$$

Proof. From the trigonometric identity $\cos(\omega\tau) = \cos(\omega\tau + 2k\pi)$, we derive

$$\tau_0^{(k)} = \frac{1}{w_0}\left[\arccos\cos\left(-\frac{K_1 \times K_3 + K_2 \times K_4}{K_3^2 + K_4^2}\right) + 2k\pi\right], \quad k = 0, 1, 2, \ldots, \tag{14}$$

We then obtain $\tau_0 = \min\left\{\tau_0^{(k)}\right\} = \tau_0^{(0)}$.

Differentiating both sides of Equation (10) with respect to τ, we arrive at the following equality.

$$\left(\frac{ds}{d\tau}\right)^{-1} = \frac{B_1'(s)e^{s\tau} + B_2'(s)}{sB_2(s)} - \frac{\tau}{s}. \tag{15}$$

Substituting $\tau = \tau_0$ and $s = i\omega_0$ into equation (15), we obtain the following expression.

$$\left(\frac{ds}{d\tau}\right)^{-1} = \frac{i\Theta_1 + \Theta_2}{i\Theta_3 + \Theta_4} - \frac{\tau_0}{iw_0}, \tag{16}$$

where

$$\begin{aligned}
\Theta_1 &= \mathrm{Re}\left[B_1'(i\omega_0)\right]\sin(\omega_0\tau_0) + \mathrm{Im}\left[B_1'(i\omega_0)\right]\cos(\omega_0\tau_0) + \mathrm{Im}\left[B_2'(i\omega_0)\right],\\
\Theta_2 &= \mathrm{Re}\left[B_1'(i\omega_0)\right]\cos(\omega_0\tau_0) - \mathrm{Im}\left[B_1'(i\omega_0)\right]\sin(\omega_0\tau_0) + \mathrm{Re}\left[B_2'(i\omega_0)\right],\\
\Theta_3 &= \omega_0\mathrm{Re}[B_2(i\omega_0)],\\
\Theta_4 &= -\omega_0\mathrm{Im}[B_2(i\omega_0)].
\end{aligned}$$

The real part of Equation (16) is given by

$$\mathrm{Re}\left(\frac{ds}{d\tau}\right)^{-1} = \frac{\Theta_1\Theta_3 + \Theta_2\Theta_4}{\Theta_3^2 + \Theta_4^2}. \tag{17}$$

Moreover, we verify that the purely imaginary root $s = i\omega_0 e^{i\pi/(2\alpha)}$ is simple. Define the characteristic function $F(s, \tau) = B_1(s) + B_2(s)e^{-\tau s}$. Since $B_2(i\omega_0) \neq 0$ and $s \neq 0$, we have $\partial F/\partial\tau = -sB_2(s)e^{-\tau s} \neq 0$ at the critical point. By the implicit function theorem,

$\left(\frac{ds}{d\tau}\right)^{-1} = \frac{\partial F/\partial s}{\partial F/\partial \tau}$. Equation (16) shows that $(ds/d\tau)^{-1}$ is a well-defined finite complex number under (H_4), which implies $\partial F/\partial s \neq 0$. Therefore, the purely imaginary characteristic root is simple.

Under Assumption (H_4), the expression in Equation (17) is positive. Since the imaginary axis corresponds to $|\arg(s)| = \pi/2 > \alpha\pi/2$ for $\alpha < 1$, the crossing of the imaginary axis implies that the characteristic roots enter the region $|\arg(s)| < \alpha\pi/2$, so that the fractional-order spectral condition is violated and E^* loses stability. This gives rise to a Hopf bifurcation, and the corresponding transversality condition for Hopf bifurcation is satisfied. The proof is complete. □

In summary, the four standard ingredients for a Hopf bifurcation are satisfied as follows: (1) Existence of a purely imaginary root: Under (H_3), Proposition 1 guarantees a positive root h_0 of $f(h) = 0$, yielding purely imaginary roots at $\tau = \tau_0$. (2) Simplicity of the root: As shown above, (H_4) ensures $\partial F/\partial s \neq 0$ at $(i\omega_0, \tau_0)$, so the root is simple. (3) Stability before bifurcation: Under (H_1) and (H_2), the system is asymptotically stable at $\tau = 0$ (Theorem 4). (4) Nonzero transversality: Under (H_4), Lemma 3 establishes $\mathrm{Re}[ds/d\tau]_{\tau=\tau_0} > 0$, so the roots cross the imaginary axis transversely from the stable to the unstable half-plane.

We therefore draw the following main conclusions:

Theorem 5. *Suppose assumptions* (H_1)–(H_4) *all hold. Then the following statements hold:*
(i) For $\tau \in [0, \tau_0)$*, system (2) is locally asymptotically stable at the equilibrium* E^**.*
(ii) At $\tau = \tau_0$*, a Hopf bifurcation emerges at* E^* *for system (2).*
(iii) For $\tau \in (\tau_0, +\infty)$*, the equilibrium* E^* *loses stability.*

4. Numerical Simulations

In this section, numerical simulations of system (2) are carried out via the Adams–Bashforth–Moulton method. Throughout the numerical simulations, a fixed step size $h = 0.01$ is used, the simulation horizon is set to $t \in [0, 100]$, and the history functions are initialized as $\phi_i(\theta) = 0.1$ for $\theta \in [-\tau, 0]$ in accordance with (3). In addition, three typical fractional orders, namely $\alpha = 0.90$, 0.95, and 1.00, are adopted for comparative analysis, where the integer-order case $\alpha = 1$ serves as a special scenario of fractional calculus. This comparative simulation reveals essential differences between fractional-order and integer-order dynamical models and illustrates that fractional-order frameworks are well suited to capture memory-dependent dynamical behaviors. Furthermore, the influence of time delay on the integer-order system is analyzed by comparing the numerical results in Figures 2 and 3. Numerical results show that the system can regain stability at an originally unstable time-delay parameter τ by adjusting the fractional order. This phenomenon demonstrates that the Hopf bifurcation point varies with the fractional order, which further changes the stability domain of the system. To intuitively and quantitatively illustrate such order-dependent dynamical transitions, several valuable conclusions on stability switching induced by fractional order variations are drawn accordingly. By assigning specific values to the parameters of system (2), we obtain the following system:

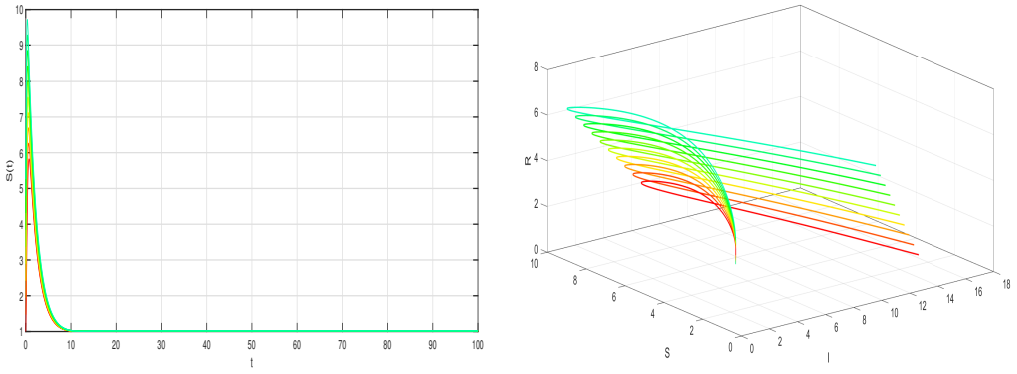
$$\begin{cases} D^{\alpha} I(t) = 1 - \dfrac{0.79 I(t-\tau) S(t-\tau)}{1 + 0.1 S(t-\tau)} - 0.2 I(t), \\ D^{\alpha} S(t) = \dfrac{0.7 \times 0.79 I(t-\tau) S(t-\tau)}{1 + 0.1 S(t-\tau)} - 0.3 S(t) - 0.2 S(t), \\ D^{\alpha} R(t) = \dfrac{(1-0.7) \times 0.79 I(t-\tau) S(t-\tau)}{1 + 0.1 S(t-\tau)} + 0.3 S(t) - 0.2 R(t). \end{cases}$$

Through direct calculations, we obtain the rumor-spreading equilibrium point $E^* = (I^*, S^*, R^*)$, where

$$I^* \approx 1.003, \quad S^* \approx 1.092, \quad R^* \approx 2.808.$$

This rumor-spreading equilibrium is obtained by setting all time derivatives of the dynamical system to zero according to the equilibrium definition. Through successive algebraic substitution and simplification of the resulting algebraic equations, we arrive at this explicit closed-form expression for the rumor-spreading equilibrium point.

We first perform numerical verification for the delay-free integer-order case $\alpha = 1$. As shown in Figure 2a, the system converges rapidly to a stable equilibrium when no time delay is introduced. Figure 2b displays the corresponding phase portrait, which verifies the stability of system (2) at this equilibrium.

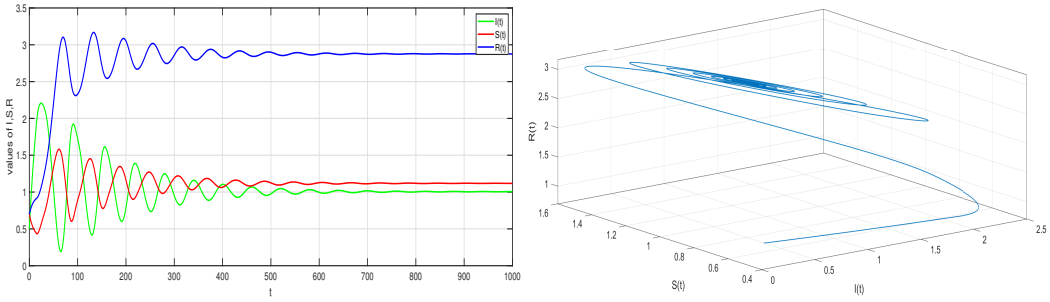


(**a**) (**b**)

Figure 2. The diagram of local asymptotic stability for system (2) at E^* in the case of $\alpha = 1$ and $\tau = 0$. Panel (**a**) shows that $S(t)$ converges to its equilibrium value, illustrating the local asymptotic stability of E^* for $\alpha = 1$ and $\tau = 0$. Panel (**b**) shows that $S(t)$, $I(t)$ and $R(t)$ converge to the equilibrium E^*, illustrating its local asymptotic stability for $\alpha = 1$ and $\tau = 0$.

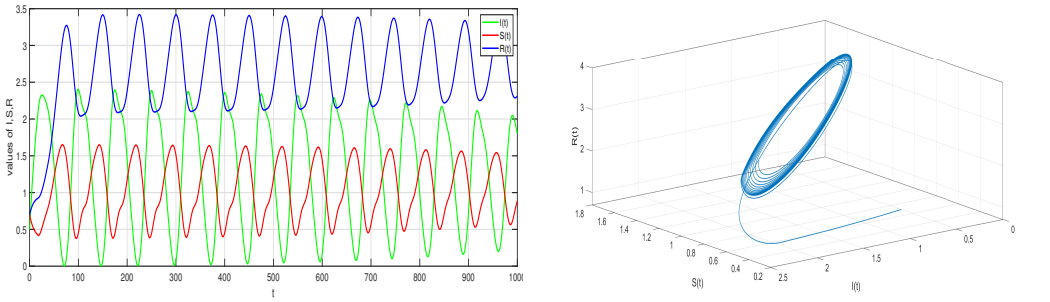
For the integer-order model with $\alpha = 1$, numerical computations yield a Hopf bifurcation critical point at $\tau_0 = 3.19$. When $\tau < \tau_0$, Figure 3a shows that the system still converges to its equilibrium, albeit at a markedly slower rate than in the delay-free case in Figure 2a. This indicates that time delay weakens system stabilization; specifically, susceptible, spreading, and recovered individuals in social network systems require a longer time to reach steady-state equilibrium. This stability characteristic is further verified by the stable three-dimensional ISR phase portrait in Figure 3b. In contrast, for $\tau > \tau_0$, Figure 4a presents persistent large-amplitude oscillations in the system trajectories, and Figure 4b displays a clear limit cycle in the ISR phase space, which confirms the loss of system stability. These numerical results are consistent with the theoretical analysis: the system remains locally asymptotically stable for $\tau < \tau_0$ and becomes unstable once the time delay exceeds the critical threshold τ_0.

For the fractional-order model with $\alpha = 0.95$, numerical computations identify the Hopf bifurcation critical point at $\tau_1 = 3.83$. For $\tau < \tau_1$, Figure 5a illustrates that the system converges to a stable equilibrium, and Figure 5b further verifies system stability via the ISR phase portrait, where all trajectories asymptotically converge to the unique equilibrium. In contrast, when $\tau > \tau_1$, Figure 6a shows persistent large-amplitude oscillations of the system state variables, and Figure 6b presents a distinct limit cycle in the ISR phase space, which demonstrates the instability of the system. Numerical results verify that the system maintains local asymptotic stability for $\tau < \tau_1$ and loses stability for $\tau > \tau_1$, which is in good agreement with the theoretical conclusions.



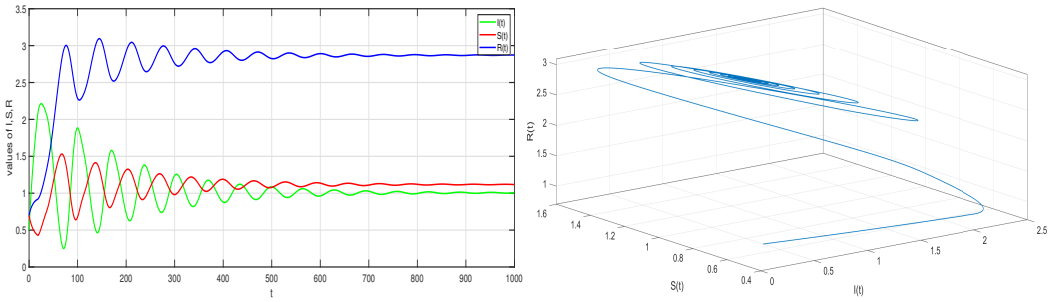
(**a**) (**b**)

Figure 3. Under the parameter settings $\alpha = 1$, $\tau = 3$, system (2) is locally asymptotically stable at E^*. Panels (**a**,**b**) show that $S(t)$, $I(t)$ and $R(t)$ converge to E^* for $\alpha = 1$ and $\tau = 3$, illustrating the local asymptotic stability of E^*.



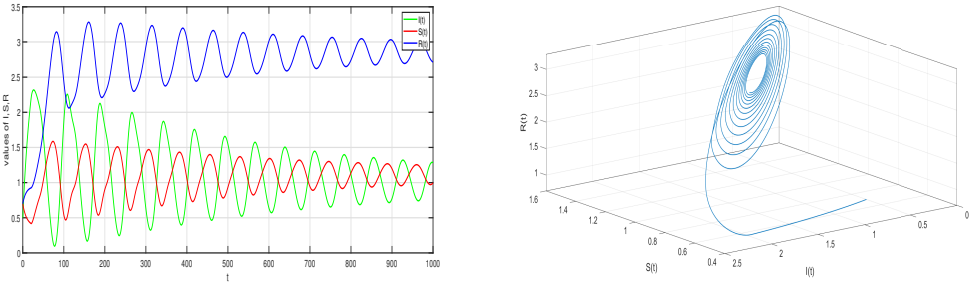
(**a**) (**b**)

Figure 4. When $\alpha = 1$, $\tau = 3.5$, system (2) displays instability at E^*. Panels (**a**,**b**) show that $S(t)$, $I(t)$ and $R(t)$ do not converge to E^* for $\alpha = 1$ and $\tau = 3.5$, illustrating the instability of E^*.



(**a**) (**b**)

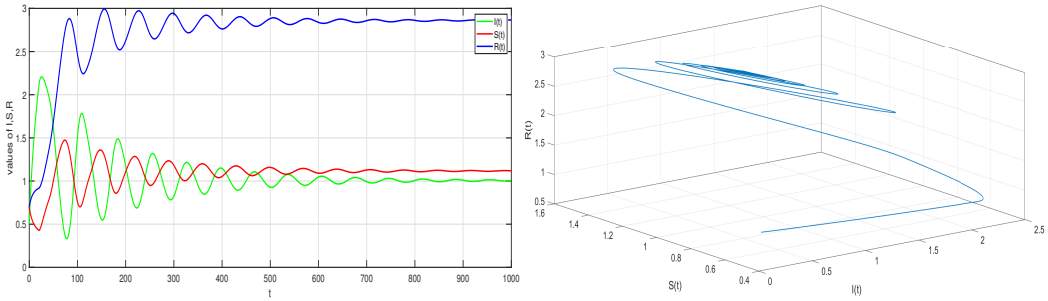
Figure 5. For $\alpha = 0.95$, $\tau = 3.5$, system (2) displays local asymptotic stability at E^*. Panels (**a**,**b**) show that $S(t)$, $I(t)$ and $R(t)$ converge to E^* for $\alpha = 0.95$ and $\tau = 3.5$, illustrating the local asymptotic stability of E^*.



(**a**) (**b**)

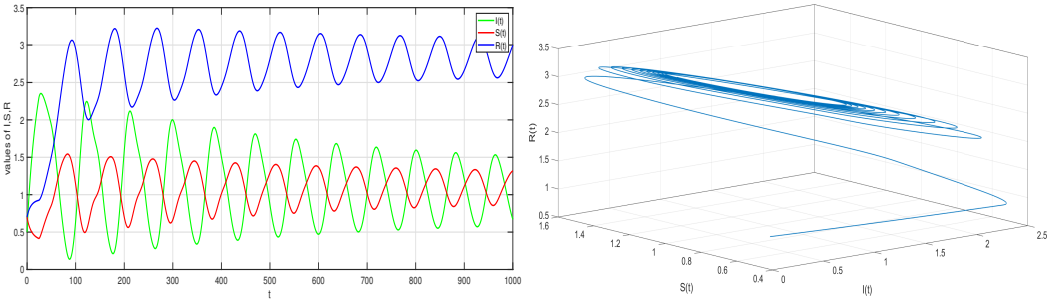
Figure 6. When $\alpha = 0.95$, $\tau = 4$, system (2) displays instability at E^* . Panels (**a**,**b**) show that $S(t)$, $I(t)$ and $R(t)$ do not converge to E^* for $\alpha = 0.95$ and $\tau = 4$, illustrating the instability of E^*.

For the fractional-order model with $\alpha = 0.90$, numerical computations locate the Hopf bifurcation critical point at $\tau_2 = 4.49$. For $\tau < \tau_2$, Figure 7a shows that the system converges to a stable equilibrium, and Figure 7b confirms this stability through the ISR phase portrait, in which all system trajectories converge to a fixed equilibrium point. In contrast, for $\tau > \tau_2$, Figure 8a presents sustained large-amplitude oscillations of the state variables, while Figure 8b displays a clear limit cycle in the phase space, which verifies the instability of the system. Numerical simulations demonstrate that the system is locally asymptotically stable for $\tau < \tau_2$ and unstable for $\tau > \tau_2$, which is fully consistent with the theoretical predictions.



(**a**) (**b**)

Figure 7. For $\alpha = 0.90$, $\tau = 4$, system (2) displays local asymptotic stability at E^*. Panels (**a**,**b**) show that $S(t)$, $I(t)$ and $R(t)$ converge to E^* for $\alpha = 0.9$ and $\tau = 4$, illustrating the local asymptotic stability of E^*.



(**a**) (**b**)

Figure 8. When $\alpha = 0.90$, $\tau = 4.8$, system (2) displays instability at E^*. Panels (**a**,**b**) show that $S(t)$, $I(t)$ and $R(t)$ do not converge to E^* for $\alpha = 0.9$ and $\tau = 4.8$, illustrating the instability of E^*.

To further verify the above theoretical results, we plot the Hopf bifurcation diagrams of system (2) under different fractional orders, as illustrated in Figure 9. Figure 9A–C depict the stability evolution of system (2) with respect to the bifurcation parameter for $\alpha = 0.90$, 0.95, 1.00.

Figure 10 presents the Hopf bifurcation curves of system (2) for fractional orders α = 0.90, 0.95 and 1.00. Each data point in Figure 10 represents the critical Hopf bifurcation threshold under the corresponding fractional order. The area beneath these bifurcation points corresponds to the stable domain of system (2), whereas the region above represents the unstable domain.

To further validate the theoretical predictions, Table 2 reports the critical frequencies ω_0 and the critical delays obtained from both the characteristic equation and the numerical simulations. The theoretical values are computed by solving Equation (13) for the smallest positive root h_0, recovering $\omega_0 = h_0^{1/\alpha}$, and evaluating $\tau_0 = \arg[-B_1(i\omega_0)/B_2(i\omega_0)]/\omega_0$. The numerical values are the bifurcation thresholds identified from the onset of sustained oscillations in the time-domain simulations (Figures 4, 6 and 8). The limit cycles observed in Figures 4, 6 and 8) occur at delay values that exceed the theoretically predicted critical

thresholds τ_0, τ_1, and τ_2 (see Table 2), confirming that these oscillations are the manifestation of the Hopf bifurcation established in Theorem 5, rather than arbitrary transient behavior.

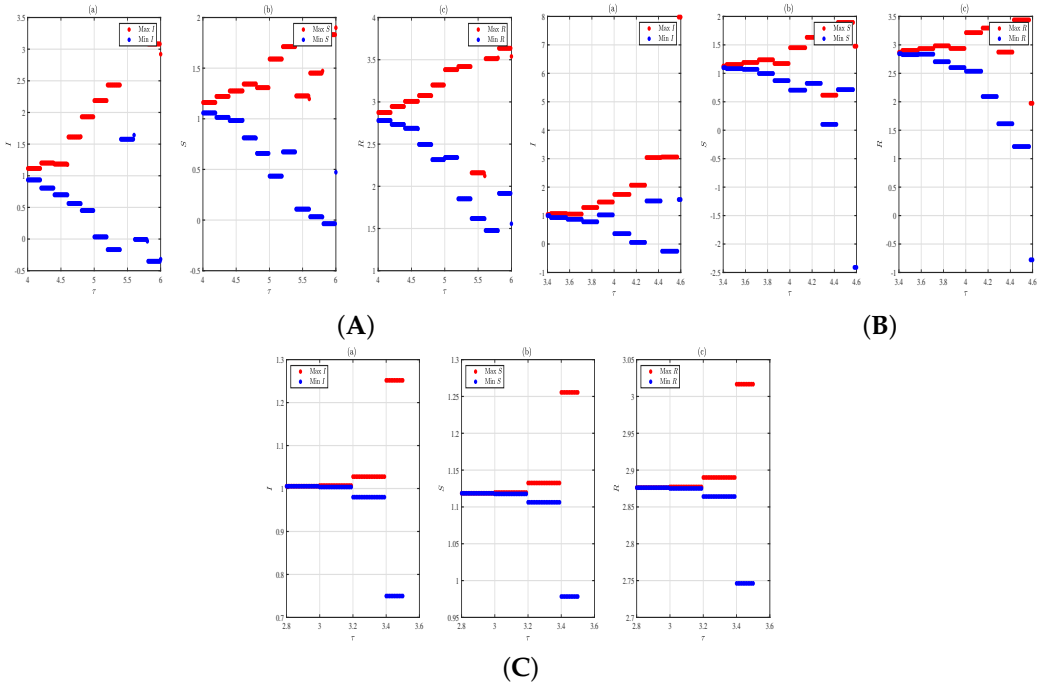


Figure 9. The bifurcation diagrams of model (2) for $\alpha = 0.90$, 0.95 and 1.00. Panels (**A**–**C**) correspond to $\alpha = 0.90$, $\alpha = 0.95$ and $\alpha = 1.00$, respectively; in each panel, subfigures (**a**–**c**) display the bifurcation diagrams of $S(t)$, $I(t)$ and $R(t)$, respectively.

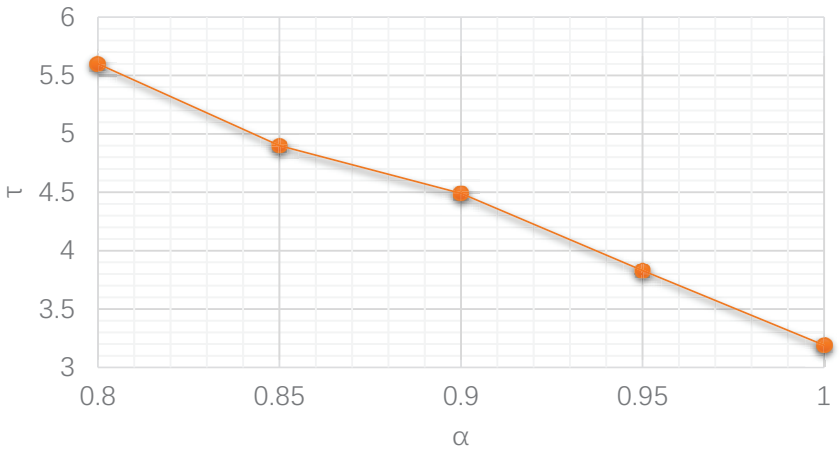


Figure 10. How the fractional-order sequence affects the bifurcation point τ_i (i = 0, 1, 2).

Table 2. Comparison of theoretical and numerical critical delays for different fractional orders.

α	ω_0	τ_{theory}	τ_{num}	Relative Error
1.00	0.466	3.661	3.19	14.8%
0.95	0.433	4.170	3.83	8.9%
0.90	0.399	4.763	4.49	6.1%

Remark 5. *Comparisons between Figures 4 and 5 indicate that we only adjust the fractional order while keeping the delay parameter τ fixed. Further comparisons of Figures 6 and 7 show that varying the fractional order can switch the system from an unstable state to local asymptotic stability, which implies a remarkable expansion of the stability domain. Combining the three aforementioned cases,*

we extract all critical bifurcation thresholds from Figure 9 to produce Figure 10. Figure 10 clearly illustrates that the critical bifurcation value declines monotonically as the fractional order α rises, which in turn shrinks the system's stability domain.

Remark 6. *From the above numerical simulations, we derive the critical bifurcation thresholds* τ_i $(i = 0, 1, 2)$ *for system (2). The numerical results demonstrate that for a fixed fractional order, the system is locally asymptotically stable if* $\tau < \tau_i$ *and loses stability if* $\tau > \tau_i$*, which verifies Theorem 3. Moreover, the size of the system's stability domain depends on the fractional order: lowering the fractional order raises the critical bifurcation value* τ_i *and greatly enlarges the stability domain. Accordingly, when modeling practical real-world phenomena, tuning the fractional order provides a flexible way to capture memory-related dynamical features of the system.*

5. Conclusions

This paper mainly discusses the dynamical behavior of a fractional-order ISR rumor propagation model with time delay. The model incorporates a Holling-type II saturated incidence rate to characterize the saturation effect dependent on the density of spreaders, such as the dispersion of audience attention caused by an excessive number of rumor spreaders. We assume that when rumor spreaders propagate rumors to ignorant individuals, the state of ignorant individuals will inevitably change: they either become spreaders or removers.

By calculating the equilibrium points of the model, this paper proves the local asymptotic stability of the rumor-free equilibrium. Theorems are derived using methods such as the Laplace transform, fractional-order stability criteria, and transversality conditions. Through calculations, the bifurcation points τ_i of the model are obtained. The model is locally asymptotically stable when $\tau < \tau_i$ and unstable when $\tau > \tau_i$.

In numerical simulations, we find that with τ kept constant, the state of the model varies under different fractional orders. Different fractional orders correspond to different bifurcation points; moreover, as the fractional order increases, the bifurcation point decreases, and the stability domain of the model gradually shrinks. The fractional order is inversely proportional to the size of the model's stability domain. These results illustrate a quantitative difference between the fractional-order and integer-order stability thresholds under the chosen parameter setting, as well as the potential flexibility of fractional-order formulations in capturing memory-dependent dynamics, and provide a theoretical reference for the control and governance of rumors.

While the present work concentrates on theoretical dynamical analysis via hypothetical numerical examples, further validation using real-world rumor datasets is highly desirable. Unfortunately, public empirical datasets containing complete compartmental time-series and rumor-fermentation time-delay measurements remain scarce. Data-driven parameter calibration and practical verification of our model will be considered in our future research.

Moreover, the present model has several limitations that outline directions for future work. First, the model uses a single discrete time delay and a Caputo fractional derivative; incorporating distributed delays, multi-delay structures, or alternative fractional operators (e.g., Atangana–Baleanu) would broaden its applicability. Second, the numerical parameters are illustrative and have not been calibrated against empirical rumor propagation data; data-driven parameter estimation remains necessary. Third, the model does not incorporate network topology or social reinforcement mechanisms; extending the analysis to complex networks with heterogeneous nodal degrees is a natural next step. Fourth, a systematic sensitivity and uncertainty analysis across the full parameter space, together with optimal control strategies for rumor mitigation, will be pursued in future research.

https://doi.org/10.3390/fractalfract10100708

Author Contributions: Conceptualization, A.M. and Y.N.; methodology, A.M.; software, Y.N.; validation, A.M. and Y.N.; formal analysis, A.M. and Y.N.; writing—original draft preparation, A.M. and Y.N.; writing—review and editing, A.M. and Y.N.; supervision, A.M. All authors have read and agreed to the published version of the manuscript.

Funding: This research is supported by the Natural Science Foundation of Xinjiang Uygur Autonomous Region, China (grant no. 2025D01C41).

Data Availability Statement: The original contributions presented in this study are included in the article. Further inquiries can be directed to the corresponding author.

Conflicts of Interest: The authors declares that they have no competing interests.

References

1. Peterson, W.A.; Gist, N.P. Rumor and public opinion. *Am. J. Sociol.* **1951**, *57*, 159–167. [CrossRef]
2. Zhao, Z.; Liu, Y.; Wang, K. An analysis of rumor propagation based on propagation force. *Phys. A Stat. Mech. Its Appl.* **2016**, *443*, 263–271. [CrossRef]
3. Pan, W.; Yan, W.; Hu, Y.; He, R. Dynamic analysis of a SIDRW rumor propagation model considering the effect of media reports and rumor refuters. *Nonlinear Dyn.* **2023**, *111*, 3925–3936. [CrossRef]
4. Yin, F.; Jiang, X.; Qian, X.; Xia, X.; Pan, Y.; Wu, J. Modeling and quantifying the influence of rumor and counter-rumor on information propagation dynamics. *Chaos Solitons Fractals* **2022**, *162*, 112392. [CrossRef]
5. Teodoro, G.S.; Machado, J.A.T.; Oliveira, E.C.D. A review of definitions of fractional derivatives and other operators. *J. Comput. Phys.* **2019**, *388*, 195–208. [CrossRef]
6. Farman, M.; Jami, K.; Nisars, K.S.; Ahmad, H.; Sambas, A. Predictive behavior of globally rumour propagation using a fractional order a time scale dynamical model with synthetical social factors. *J. Appl. Math. Comput.* **2026**, *71*, 4761–4786 [CrossRef]
7. Ye, Y.; Zhou, J. Spatiotemporal pattern evolution on a spatial fractional Rosenzweig-MacArthur model. *Ric. Mat.* **2025**, *74*, 3009–3033. [CrossRef]
8. We, Z. Dynamic fractional-order ISDR rumor propagation model incorporating refutation mechanism in complex networks. *Sci. Rep.* **2025**, *15*, 31137. [CrossRef] [PubMed]
9. Niu, Y.; Muhammadhaji, A. Dynamics of a fractional-order IDSR rumor propagation model with time delays. *Fractal Fract.* **2025**, *9*, 242. [CrossRef]
10. Ye, M.; Li, J.; Han, X.; Jiang, H. Global analysis of a fractional-order reaction-diffusion rumor-spreading model in multi-lingual environment. *Eur. Phys. J. Plus* **2023**, *138*, 102. [CrossRef]
11. Hou, H.; Wang, Y.; Zhai, Q.; Sun, X. Optimal control of stochastic fractional rumor propagation model in activity-driven networks. *Appl. Math. Model.* **2025**, *142*, 115968. [CrossRef]
12. Zhao, L.; Cui, H.; Qiu, X.; Wang, X.; Wang, J. SIR rumor spreading model in the new media age. *Phys. A Stat. Mech. Its Appl.* **2013**, *392*, 995–1003. [CrossRef]
13. Petrš, I. *Fractional-Order Nonlinear Systems: Modeling, Analysis and Simulation*; Springer Science & Business Media: Berlin/Heidelberg, Germany, 2011.
14. Deng, W.; Li, C.; Lv, J. Stability analysis of linear fractional differential system with multiple time delays. *Nonlinear Dyn.* **2007**, *48*, 409–416. [CrossRef]
15. Zhou, T.; Muhammadhaji, A. Dynamics in a fractional-order competitive-competitive-cooperative system with Beddington-DeAngelis functional responses and delay. *Fractal Fract.* **2026**, *10*, 176. [CrossRef]
16. Bhalekar, S.; Daftardar-Gejji, V. A predictor-corrector scheme for solving nonlinear delay differential equations of fractional order. *J. Fract. Calc. Appl.* **2011**, *1*, 1–9.
17. Alhamzi, G.; Singh, R.; Dubey, R.S.; Mishra, M.N. Analytical study of a fractional smoking epidemic model: A comparative study via Yang-Abdel-Cattani and Atangana-Baleanu derivative with Sumudu transform. *Fractal Fract.* **2026**, *10*, 385. [CrossRef]
18. Sharma, R.; Goswami, P.; Dubey, R.S.; Belgacem, F. A new fractional derivative operator and its application to diffusion equation. *Math. Methods Appl. Sci.* **2023**, *46*, 16562–16573. [CrossRef]

Disclaimer/Publisher's Note: The statements, opinions and data contained in all publications are solely those of the individual author(s) and contributor(s) and not of MDPI and/or the editor(s). MDPI and/or the editor(s) disclaim responsibility for any injury to people or property resulting from any ideas, methods, instructions or products referred to in the content.